Virtual sensing for strain estimation in wind turbine support structures based on a biaxial accelerometer

Answer to the reviewer's comments

The authors would like to thank the editor and reviewers for their time and effort to review the article and for their constructive and relevant comments. We appreciate the chance to clarify the addressed points. This will undoubtedly help in improving the quality of the manuscript. The article is revised according to the reviewers' remarks and queries, with detailed responses and explanations of the edits given below. Edits in the manuscript have been highlighted in red color for the first reviewer (Report #1) and in blue color for the second reviewer (Report #2). We note that during the revision, the number of lines has been changed. Therefore, in the proceeding paragraphs, we refer to the revised article.

Report #1

The authors thank the reviewer for their feedback. As no revision was suggested, no changes were made in the manuscript based on Report #1.

Report #2

The topic of the paper is of high importance, as the possibility of estimating strains from accelerations enables a continuous assessment of fatigue consumption based on a monitoring setup that is easy to install and cost-effective.

The paper is well structured, including a clear description of the methodology, its validation through a simple laboratory experiment and a final validation using data collected in an offshore wind turbine. As acknowledged by the authors in Section 5, the proposed methodology has some relevant limitations, which make its application to utility-scale wind turbines quite challenging. Nevertheless, a balanced discussion of the methodology may still be valuable for the scientific community.

Still, the following points should be addressed:

We thank the reviewer for their feedback. We have taken your comments into account and changed the manuscript accordingly. The changes are explained in detail below.

Figure 1:

- **The effect of the low-pass filter is not clearly visible in the presented spectra. A sudden change in amplitude at the cut-off frequency would be expected, as observed for the high-pass filter.**

  The authors agree, that the effect of low-pass filtering is not clearly visible. We updated the figure and use zero-phase fourth-order Butterworth filters with a cutoff frequency of 0.1 Hz. Furthermore, we indicated the approximate eigenfrequency obtained from an FE model of the support structure.

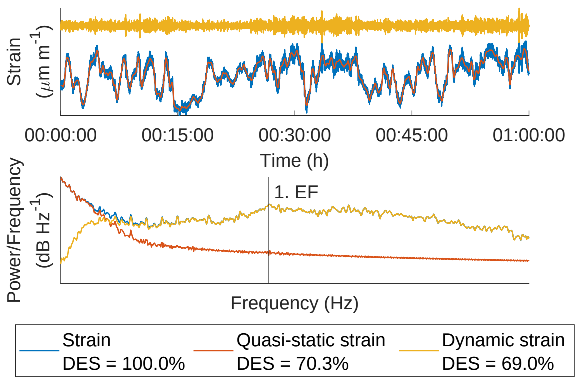

Figure 1: Strain time series of an offshore wind turbine tower under partial load operation. The low-pass and high-pass filtered signals were obtained using zero-phase fourth-order Butterworth filters with a crossover frequency of 0.1 Hz. The first bending eigenfrequency (EF) of the tower is indicated. The damage equivalent strain (DES) is normalised with respect to the total DES of the unfiltered signal.

Additionally we changed the following paragraph (page 3 line 76):

If the quasi-static component of the strain set here to below 0.1 Hz is neglected, the fatigue damage, expressed here via the damage equivalent strain (DES), is significantly underestimated, only adding up to about 69 % of the actual DES.

Section 2.1:

- **In the presented equations and in the integration filter shown in Figure 4, it is assumed that m does not depend on frequency. However, m varies with the shape of the dominant mode at each frequency. Therefore, Equation (4) is only valid for frequencies close to zero.**

  The authors agree with the reviewer's statement. However, as the influence of the tilt error is most pronounced close to the static case and hardly influences higher frequencies as visible in Fig. 4, the assumptions of a constant m is regared as valid by the authors. Using a frequency-dependent m only causes minor changes in the combined integration and tilt error compensation for frequencies, in which the tilt error is present (below the first eigenfrequency) as visible the Figure below (not included in the manuscript). Taking into account a theoretically frequency dependent tilt constant can however cause problems for frequencies, in which the assumed excitation causes $w = 0$ in $m = \frac{w'}{w}$, resulting in a pole in the combined integration and tilt error compensation filter as visible on the right side of the Figure below.

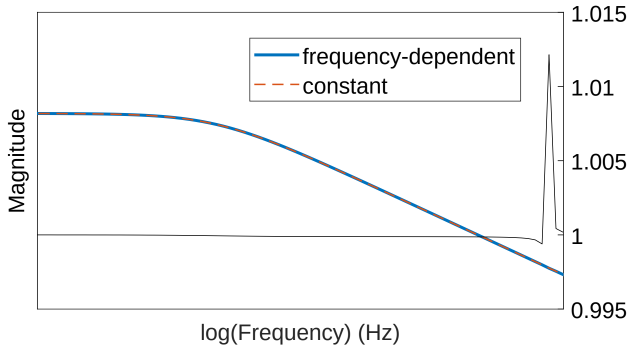

Figure 2: Combined integration and tilt error compensation filter using a frequency-dependent tilt constant m and a constant m from the static case. Additionally, the deviation is shown on the right axis.

We updated the manuscript accordingly (page 7 lines 164-172). Please notice that the section has been shortened due to the reviewer's comments:

In previous work by Jonscher et al. 2025, it was found that the measured acceleration a_{meas} is corrupted by gravitational acceleration g, resulting in a share of the measured acceleration, which is caused by g ($a_g(f)$) due to the tilt of the sensor as illustrated in Fig. 3. The actual acceleration of the structure in the inertial coordinate frame $a_{str}(f)$ can be expressed as

$$a_{str}(f) = a_{meas}(f) - a_g(f) = a_{meas}(f)\frac{1}{(2\pi f)^{-2}\, gm + 1} = a_{meas}(f)c(f,m), \qquad (1)$$

where $c(f,m)$ is the correction factor accounting for the tilt error and m is the tilt constant. m describes the ratio between the tilt w' and the lateral displacement w in the quasi-static bending line, which is valid for small tilt angles in the quasi-static frequency range:

$$m = \frac{w'}{w}. \qquad (2)$$

- **The pitch and roll axes are not defined.**

  The authors agree that a better definition of the axes would be beneficial. We updated the manuscript accordingly (page 9 lines 210-212):

  The rotation matrix is defined such that the mean gravitational acceleration vector measured in the sensor frame is aligned with the negative y-axis. To two Euler angles ϕ and ξ represent a rotation about the sensor x-axis and z-axis, respectively

- **This section could be shortened to focus on the main points, which are summarized in Equations (10) and (11).**

  The author agree that the section can be shortened in addition to the changes above.

  Page 7 lines 173-174:

  The tilt constant m is only determined for the static case as the tilt error is neglectable in the dynamic frequency range dominated by structural eigenmodes of current wind turbines. The correction factor $c(f, m)$ has the amplitude response of a second-order high-pass filter with a cutoff frequency of gm but does not change the phase of the input signal.

  and page 8 line 187:

  The static displacement can be expressed as

$$w(f) = \frac{1}{m} w'(f) = \frac{1}{m} \frac{a_g(f)}{g} \tag{5}$$

  using Equation 2.

  and page 9 line 215:

  The Euler angles can be determined as

$$\phi = \arcsin\left(-\frac{\overline{a}_{\mathrm{raw},z}}{|\overline{\mathrm{a}}_{\mathrm{raw}}|}\right) \quad \xi = \arcsin\left(\frac{\overline{a}_{\mathrm{raw},x}}{|\overline{\mathrm{a}}_{\mathrm{raw}}| \cos\phi}\right). \tag{10}$$

Section 2.2:

- **Please explain how the continuous function presented in Figure 5 was obtained. This function depends on the structure and on the location where displacements and strains are measured.**

  The continuous function is obtained by increasing the number of supporting frequencies, for which $T_{\mathrm{w}\to\varepsilon}(f) = \frac{\varepsilon_{\mathrm{t,FE}}(f)}{w_{\mathrm{m,FE}}(f)}$ is calculated, from three to 101. It is in this sense not continuous but has a higher frequency resolution. However, similar to using a frequency-dependent tilt constant, $T_{\mathrm{w}\to\varepsilon}(f)$ can diverge for frequencies where $w_{\mathrm{m,FE}} \approx 0$, which is why we use the step function instead.

  We edited the following paragraph (page 11 lines 270-271):

  This would result in $T_{w\to\varepsilon}$ being a step function that is only correct at the eigenfrequencies and approximates the response at neighbouring frequencies, which is shown as an example in Fig. 5 for arbitrary locations of w and ε.

  and page 12 lines 277-278:

  In theory, $T_{w\to\varepsilon}$ can be constructed for every excitation frequency, resulting in the example continuous graph shown in Fig. 5, which is calculated here exemplarily for 101 excitation frequencies in the shown frequency band.

- **Furthermore, its shape is not consistent with the numerical results presented in Table 4.**

  This is correct, as the numerical results in Table 4 are calculated from an earlier version of the FE model. Additionally, we corrected a minor mistake in the calculation of the ΔDES. We updated Table 3, Table 4 and Table 5 as well as Fig. 12 and Fig. 13 in the manuscript accordingly.

  The following paragraphs have been updated.

  Page 1 line 12:

  In the laboratory experiment, both displacements and strains are estimated accurately with errors below 2.2 % and 5 %, respectively.

  and page 17 lines 367-369:

  The strain estimation consistently yields excellent results, with an absolute ΔDES below 1.7 % except for the strain estimation at MP4 using acceleration at MP2, indicating that, for a known excitation, the proposed method enables reliable strain estimation using a single accelerometer. Furthermore, spatial extrapolation of the strain is possible, as accurate strain estimation can be achieved regardless of the input and output positions.

  and page 28 lines 548-552:

  Excellent agreement between the estimated and measured displacements and strains was observed in the laboratory experiment, with deviations in the damage equivalent strain of less than 5 % across all accelerometer measurement points. Both the quasi-static and dynamic responses could be captured and a single accelerometer position was shown to be sufficient to accurately estimate strains at multiple locations. However, limited accuracy was observed close to frequency band limits, being responsible for the majority of the observed error.

Section 4:

- **It would be useful to present results for a higher frequency range, above 1 Hz.**

  The authors agree, that a the higher frequency range would also be of interest, even though for the investigated time series the vast majority of the fatigue damage is caused by vibrations in and below the first eigenfrequency. We increased the cut-off frequency to 2 Hz and recalculated all results for this frequency range. In addition to the changes in the paragraphs below we updated Fig. 16,Fig. 18 and Fig. 19 as well as Table 11. Furthermore, Table 10 was expanded to also contain the values of $T_{\mathrm{w}\rightarrow\varepsilon}$ in the second bending mode shape.

Table 10: Displacement-to-strain transmissibility function $T_{\mathrm{w}\rightarrow\varepsilon}$ in (m^{-1}) for the strain estimation at TP from the displacements at TT, TM and TP using a separate Ritz vector in the quasi-static frequency range.

	Frequency band (Hz)		
	Quasi-static	**1. EF**	**2. EF**
$T_{w(\mathrm{TT})\rightarrow\varepsilon(\mathrm{TP})}$	2.93E-04	2.91E-04	-1.35E-03
$T_{w(\mathrm{TM})\rightarrow\varepsilon(\mathrm{TP})}$	6.03E-04	6.01E-04	-5.48E-04
$T_{w(\mathrm{TP})\rightarrow\varepsilon(\mathrm{TP})}$	2.08E-03	2.07E-03	-8.35E-04

The following paragraphs were updated:

Page 19 lines 400-402:

Both accelerations and strains were sampled at 25 Hz. The temperature-corrected measurement data recorded by the strain gauges are used to validate the strain estimation.

and page 22 lines 420-431:

All acceleration and strain time series were low-pass filtered with a cutoff frequency of 2 Hz for evaluation and validation, respectively, therefore including the quasi-static frequency range, the first eigenmode and frequencies dominated by the rotor excitation and the second eigenmode. This frequency range is chosen since it allows to capture most of the fatigue-relevant vibrations. This is illustrated exemplarily for the investigated measured strain time series from dataset 1 in Table 9. 99.5 % of the DES are caused from vibrations below 2 Hz, while almost 92 % of the total DES can already be captured by the quasi-static vibrations below 0.1 Hz alone for this time series. This share increases to more than 99 % when the first eigenfrequency is included (0 - 0.5 Hz). However, it should be noted that frequencies above 2 Hz, which are dominated by the rotor dynamics and higher tower eigenmodes, can have a larger influence the fatigue loads in the support structure for other operational or environmental conditions, for example by increasing the strain amplitude during sudden events like shut-down or start-ups. Despite this, the cut-off frequency is chosen as 2 Hz allowing to focus on the performance in the low-frequency range, in which strain estimation using accelerations only is typically challenging.

Table 9: Share of damage equivalent strain caused by for different frequency bands for the measured strain time series at TP at 35°.

0 - 0.1 Hz	0 - 0.5 Hz	0 - 2 Hz	0 - 12.5 Hz
91.9 %	99.1 %	99.5 %	100 %

and page 24 lines 461-470:

The method accurately captures the general trends, i.e., the quasi-static frequency range and the structural response close to the first eigenfrequency, as shown in the spectrum in Fig. 18. The zoom in Fig. 18 further highlights the good agreement between the estimated and measured strains in the quasi-static frequency range, regardless of the accelerometer position used as input. The agreement in the quasi-static frequency range can also be observed in Zoom 1 in Fig. 16. In contrast, the spectrum reveals bad agreement for higher frequencies dominated by the rotor harmonics and higher eigenmodes, which do however have a negligible effect on the total DES for the investigated time series. The deviation for higher frequencies is likely caused by the rotor modelling as lumped mass, which has been shown to highly influence the second tower bending mode (Reinhardt et al. 2024) and leads to bad agreement between estimated and measured strain at frequencies above the first eigenfrequency (Pedersen et al. 2026).

- **Despite the very complete experimental setup, the duration of the analysed dataset is quite limited (less than one day).**

  The authors agree, that a longer time series would be beneficial. However, at the time of submission only 9.5 hours of data was made available by our industrial partner. Since then, more data has been made available, which we decided to show here in addition. While we decide to keep the previous evaluation unchanged, we added the following evaluation using measured data over one month.

  Page 1 lines 12-13:

  For the offshore wind turbine, the damage equivalent loads at the transition piece can be estimated with a mean percentage error of below 9 %.

  and page 20 lines 403-407:

  Two datasets using the same measurement setup have been evaluated here. The first dataset encompassed 9.5 hours of continuous measurement. The second dataset encompasses one month of measurement data. The turbine operates under part-load conditions during the measurement period of dataset 1 except for approximately 20 min from 05:00 h to 05:20 h, when the turbine is shut down. The minimum, maximum and mean values of some of the relevant SCADA data are given in Table 7 for both datasets to give an impression of the occurring environmental and operational conditions (EOCs), underlining the fact that the method is applied to data under varying EOCs.

Table 7: Statistical properties of selected EOCs during the measurement period.

Quantity	Dataset 1 (9.5 hours) Min	Max	Mean	Dataset 2 (1 month) Min	Max	Mean
Wind Speed (m/s)	4.00	9.69	6.14	0.09	29.3	7.10
Yaw Angle (°)	236	312	276	0	360	-
Rel. Power (%)	0.1	55.8	17.6	0.0	100	23.5

and page 22 line 440:

The values of $T_{w \to \varepsilon}$ in this frequency range are therefore determined from the static bending line resulting from a horizontal force applied to the top of the tower, regardless of the direction and operational condition.

and page 23 line 454:

The resulting ΔDES for dataset 1 are shown in Table 11 and range from -0.53% to -10.33%.

and page 24 lines 476-485:

After having shown good accuracy for the short measurement period of dataset 1, the method has been applied to dataset 2 to assess the method's performance over a longer measurement period of one month under varying EOC. In contrast to the previous evaluation, the strain has been estimated for 10-min periods to allow for a yaw-transformation using the available 10-min mean yaw position. To avoid the observed effects of the low-pass filtering, an additional 60 minutes have been evaluated before and after the respective 10-min period and cut-off before calculating ΔDES. Both the estimated and measured strain time series have been band-pass filtered between 0.1 mHz and 2 Hz. Fig. 20 shows the results of the application of the strain estimation method to dataset 2 for the level TP in fore-aft (FA)- and side-side (SS)-direction. Additionally, Fig. 20 shows the coefficient of determination R^2 and the mean percentage error (MPE). The results show a very good agreement in FA and SS direction with only small deviations from a perfect fit as indicated by $R^2 \approx 1$ and a MPE below 9 %.

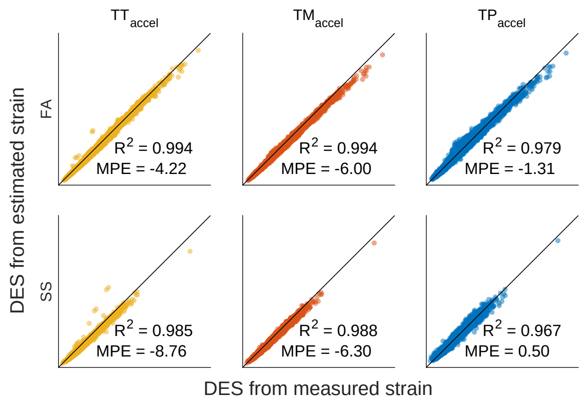

Figure 20: Scatter plot of the DES calculated from the estimated and measured strain time series in dataset 2 (one month of measurement) at TP in FA- and SS-direction using different acceleration sensors as input. Each point represents 10 minutes of measurements. The coefficient of determination R^2 and the mean percentage error (MPE) in % are given.

- **It is assumed that all loads applied to the tower can be represented by a point load at the tower top. While this assumption may be reasonably adequate for the fore–aft (FA) direction, it is not appropriate for the side–side (SS) direction. Consequently, the strains estimated for strain gauges that are less aligned with the FA direction at each time instant are likely to be less accurate.**

  The authors agree that different load assumption might be necessary for accurate strain estimation in FA- and SS-direction. However, the additional evaluation using dataset 2 shows comparable results in FA and SS direction, even though the results in FA-direction are slightly better, indicating that the load assumption are sufficiently accurate in the investigated measurement period. Although less important than in FA-direction, a share of the rotor thrust is acting in SS-direction due to yaw-misalignment. This yaw-misalignment is caused by the controller, incorrect wind vane measurements and gusts. Furthermore, within the investigated data set, other loads acting on the turbine support structure in the quasi-static frequency range like the wave loads might be small compared to the share of the rotor thrust. Different results might be observed for other locations or datasets with higher wave heights and wave peak periods further from the first eigenfrequency of the support structure.

  We edited the following paragraphs (page 25 lines 485-494):

  While both metrics indicate a slightly better estimate in FA- than in SS-direction, the observed difference in accuracy is minor. This indicates that the simplified load assumption of the thrust load being dominant regardless of the direction is sufficient for the investigated dataset for both FA and SS-direction. While the thrust load is certainly dominant in FA-direction under operation, due to yaw-misalignment (Kragh, Hansen, and Mikkelsen 2013), it appears to also be the dominant quasi-static load in SS-direction. Other loads acting on the tower like to rotor load eccentricity or the wave load do not distort the strain estimation in the investigated dataset. Furthermore in SS-direction, the quasi-static frequency range, where the load assumptions effect the estimation, is less relevant in SS-direction than in FA-direction, as a larger *share of the fatigue-relevant vibration occurs in the first eigenfrequency.*

and page 27 lines 520-524:

The dominant load varies with the direction and operational condition. While the thrust load is the dominant load in FA-direction during power production, it is less relevant in SS-direction. However, due to yaw-misalignment, the thrust load is still present in SS-direction. Additional loads from the rotor eccentricity and the waves may become relevant in SS-direction under different EOC but are neglected here.

- **Errors in DES of about 20% are quite significant, translating into a substantial error in the evaluation of the tower's fatigue life.**

  The authors agree that deviations in the DES of about 20% are significant. We discussed with the data supplier and found an error in the FE model, in which we assumed an incorrect wall thickness at the TP, where the strain gauges are installed. We updated Fig. 15, Fig. 16, Fig. 18 and Fig. 19 as well as Table 8, Table 10 and Table 11 accordingly. The deviations are now be decreased to $\leq$ 10.5%, which is similar to other relevant studies in the field suggest Fallais et al. 2025; Iliopoulos et al. 2017.

  We updated the following paragraphs (page 23 lines 454-456):

  The resulting ΔDES for dataset 1 are shown in Table 11 and range from -0.53 % to -10.33 %. This deviation is comparable to other published results in which deviations in the damage equivalent strain of around 6.1 % (Iliopoulos et al. 2017) and 2 % to 18 % (Fallais et al. 2025) have been found.

  and page 24 lines 471-474:

  Furthermore, the method shows good agreement for the shutdown event around 05:00 h, which is shown in detail in the same illustration. As shutdown events result in significant changes in strain, an accurate strain estimation is critical for fatigue estimation. Figure 19 shows the absolute error between the estimated and measured strains.

  and page 28 lines 554-556:

  The strain estimation for the offshore wind turbine also yields accurate results but shows larger variations in the damage equivalent strain, ranging from -0.5 % to -10.3 %, averaging out to a mean percentage error of less than 9 % in the validation using a month of data, which is comparable to other strain estimation methods.

References

Fallais, Dominik et al. (2025). "Long-term validation of a model-based virtual sensing method for fatigue monitoring of offshore wind turbine support structures: Comparing as-designed with state-of-the-art foundation models". In: *Marine Structures* 104, p. 103841. ISSN: 09518339. DOI: 10.1016/j.marstruc.2025.103841.

Iliopoulos, Alexandros et al. (2017). "Fatigue assessment of offshore wind turbines on monopile foundations using multi-band modal expansion // Fatigue assessment of offshore wind turbines on monopile foundations using multi–band modal expansion". In: *Wind Energy* 20.8, pp. 1463–1479. ISSN: 10954244. DOI: 10.1002/we.2104.

Jonscher, Clemens et al. (2025). "Dynamic displacement measurement of a wind turbine tower using accelerometers: tilt error compensation and validation". In: *Wind Energy Science* 10.1, pp. 193–205. DOI: 10.5194/wes-10-193-2025.

Kragh, Knud A., Morten H. Hansen, and Torben Mikkelsen (2013). "Precision and shortcomings of yaw error estimation using spinner-based light detection and ranging". en. In: *Wind Energy* 16.3, pp. 353–366. ISSN: 1099-1824. DOI: 10.1002/we.1492.

Pedersen, Mads Greve et al. (June 2026). "Performance of multi-band MDE-based virtual sensing for estimating lifetime fatigue damage equivalent loads for the IEA 15 MW reference wind turbine". English. In: *Wind Energy Science* 11.6, pp. 2053–2091. ISSN: 2366-7443. DOI: 10.5194/wes-11-2053-2026. (Visited on 06/30/2026).

Reinhardt, T et al. (June 2024). "On the influence of rotor nacelle assembly modelling on the computed eigenfrequencies of offshore wind turbines". en. In: *Journal of Physics: Conference Series* 2767.5, p. 052034. ISSN: 1742-6596. DOI: 10.1088/1742-6596/2767/5/052034. (Visited on 12/23/2025).